PERFORMANCE OF THE FIRST QDDD SPECTROGRAPH

M. Goldschmidt, D. Rieck and C.A. Wiedner
Max-Planck-Institut für Kernphysik, Heidelberg, Germany

Abstract

A new type of magnetic spectrograph for precision spectroscopy of charged particles from nuclear reaction has been put into operation. This spectrograph consists of a quadrupole followed by three dipoles, a multipole element and an electrostatic deflector. The ion optical lay-out features a point to point image in both planes and in addition an axial intermediate image. The components of the system have been mapped. After assembling the spectrograph has been ray traced with ^{3}He particles of 24 MeV. The resolving power at the full solid angle of 13 msr is $dp/p \cong 10^{-4}$ for several reactions investigated so far.

I. Introduction

Present problems in low energy nuclear spectroscopy require magnetic spectrographs with high solid angle and a resolving power of $p/dp = 10^4$ i.e. comparable to the energy stability of tandem accelerators or single-turn extraction cyclotrons. The detection of particles in the focal plane should be accomplished with position sensitive detectors - e.g. multiwire proportional chambers - to have on-line control of the measurements. Since the interest in nuclear reactions with heavy particles is steadily increasing means for correcting the kinematic broadening have to be provided.

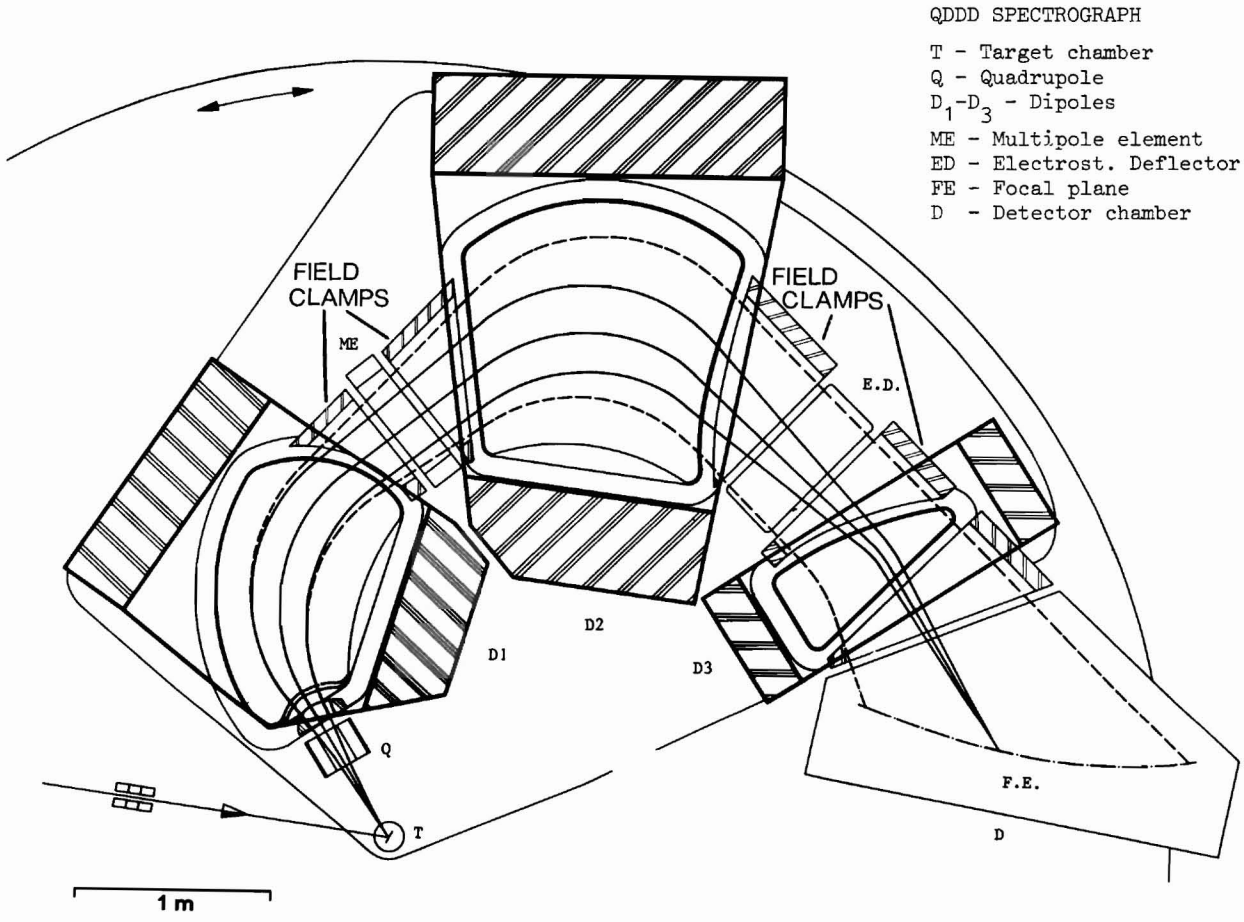

Fig. 1. Plan view of the spectrograph. With outermost particle trajectories and beam envelope of central momentum.

In detail the following specifications have been required for the spectrograph:

a) Solid angle Ω = 13 msr
b) Resolving power $p/dp = 10^4$ at the full solid angle
c) Momentum range: 80 MeV/c to 500 MeV/c
d) Simultaneously accepted momentum bite $\delta p/p$=10%
e) Dispersion D = 20 cm/% momentum bite along the focal plane
f) D/M = 10
g) Provision of a multipole element for kinematic correction up to $dp/(p \cdot d\theta)$ = 0.3/rad.

The high dispersion specified is necessary to obtain the desired resolution with on-line detectors having a spatial resolution of about 1 mm.

The criteria mentioned can be met by the new type spectrographs of the QDDD type, i.e. systems containing a quadrupole and three dipoles. These feature in addition to double focussing an intermediate axial image between the first and second dipole magnet. The method of designing intermediate image spectrographs using numerical ray tracing has been described by Enge and Kowalski.[1] Their paper also contains the details of the ion optical layout of the QDDD spectrograph, which is shown in Fig.1. To correct for aberrations curvatures up to fifth order on the pole faces had to be provided. The coefficients of these curvatures will be compared to those measured in paragraph III. Before the results of ray tracing with ^{3}He particles of 24 MeV are discussed in IV, section II, deals with some of the technological aspects.

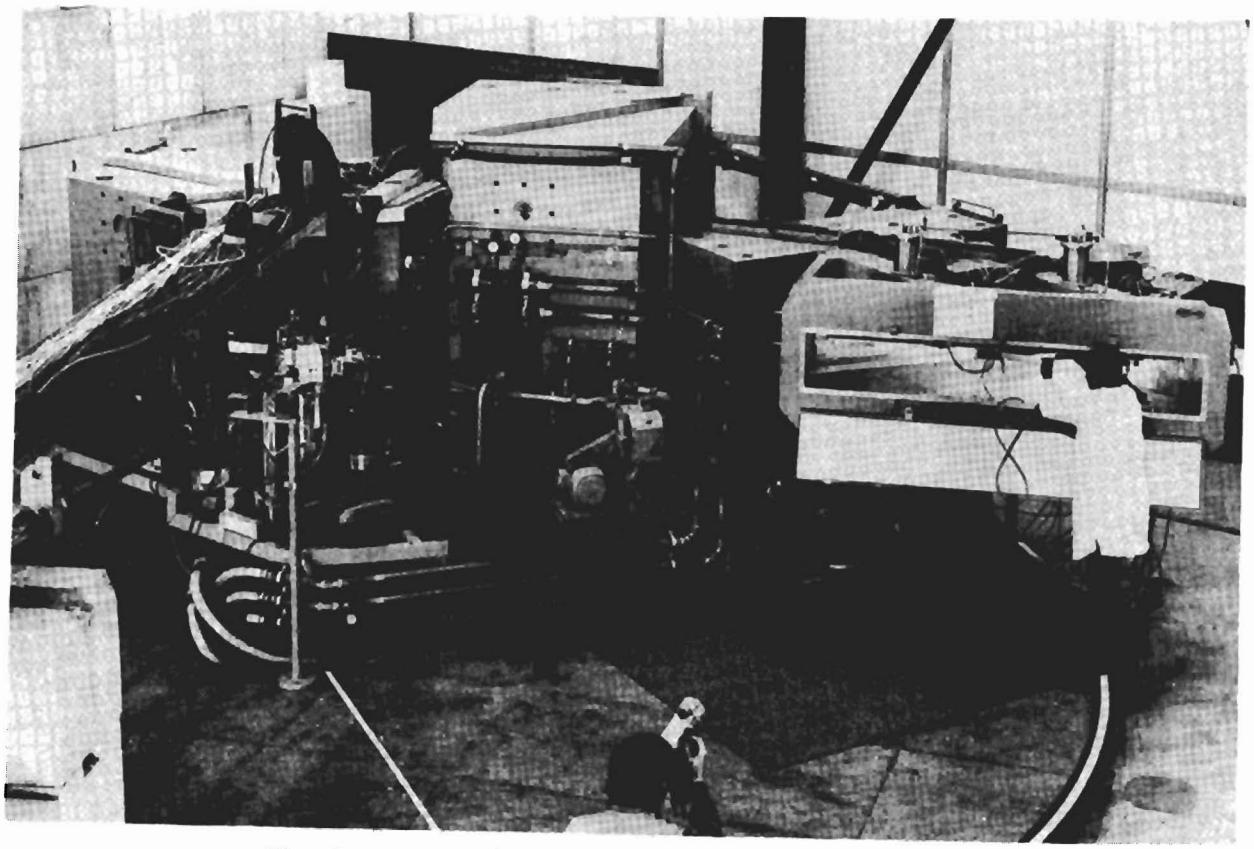

Fig. 2. General view of the spectrograph after installation.

II. Description of the Spectrograph

The first two QDDD spectrographs have been built by Scanditronix (Stockholm) for the Max-Planck-Institut für Kernphysik at Heidelberg and the Technische Hochschule München. Figure 2 shows a general view of the spectrograph after installation at Heidelberg. The main parameters are listed in Table I.

All sides of the pole pieces have approximate Rogowski contour.[2] The pole pieces are 20 cm thick and are mounted - spring loaded - into the yokes leaving a Purcell gap of 6 mm. The outermost rays of the beam are at least 2.5 gap width away from the side boundary of the pole piece.

TABLE I. Technical Specifications

Bending Radius	95 cm $\leq \rho \leq$ 105 cm
Magnetic Field	2.7 kG $\leq B \leq$ 17 kG
Total Angle of Deflection	$\phi = 180^{\circ}$
Magnet Type	H-Magnets
Quadrupole	Danby Figure-of-Eight
Magnet Pole Gap	d = 8 cm
Aperture of Quadrupole	d = 12 cm
Horizontal Acceptance	$\theta = \pm$ 55 mrd
Vertical Acceptance	$\emptyset = \pm$ 63 mrd
Length of Focal Plane	L = 2.20 m
Angular Range	$-15^{\circ} \leq \theta_S \leq +155^{\circ}$
Power Required for Max. Field	330 kW
Weight Including Support	140 tons

The pole boundaries facing the beam are milled with a computer-controlled contour cutter. It had been helpful for both, the check of the accuracy of the mechnical tolerances and the alignment and adjustment of the components with respect to each other that immediately after the milling procedure small holes were drilled into the pole pieces. For the Hall probe measurements of the fringe fields needles fitted snug into the holes. The strong nonuniformity of these was measured in the coordinate system of the field mapping machine taken on both faces of the pole piece and the data hence could be transformed to one coordinate system.

Tolerances

In order to obtain numerical values for the tolerances to be specified for the manufacturer, first order calculations with the computer program TRANSPORT have been made.[3] In each run one of the system components was shifted or turned with respect to the others and by normal matrix multiplication technique the beam trajectory was calculated through the system.

The quotient of dispersion D = 20 cm/% and resolving power R = 10^4 specifies one resolution bin width, which corresponds to 2 mm. The mechanical displacements corresponding to one bin width for the QDDD spectrograph are summarized in Table II.

The conclusions drawn from these calculations were: 1. The machining tolerances of the pole face boundaries could be relaxed to 0.2 mm. 2. The support and mounting of the components has to be sufficiently rigid to avoid deadjustments of the system, which is of course turned between experiments over long times. The latter problem has been solved by using an air cushion pad moving on a flat granite plate. Details of this support have been published elsewhere;[4] some relevant figures are: Maximum deviations of the granite plate from the plane, measured at 350 points over 66 m^2 are less than $\pm$ 0.1 mm. When turning the spectrograph the support lifts by only 0.3 mm at maximum.

TABLE II. Mechanical Displacements Corresponding to one Bin Width

System Component	Pole Face	D (mm)	ROA (deg.)	RVA (deg.)
Quadrupole	Entrance	2.33	0.50	not calc.
	Exit	1.00		
First Dipole	Entrance	0.60	1.10	0.05
	Exit	0.35		
Second Dipole	Entrance	0.30	1.46	0.11
	Exit	0.34		
Third Dipole	Entrance	0.90	1.82	0.46
	Exit	1.10		

D - Displacement along the beam axis; ROA - Rotation about optical axis; RVA-Rotation about vertical axis

Attached to the magnets are field clamps preceding each pole piece boundary. By moving off these the effective field boundary can be shifted to a certain extent, remachining them could be used to correct for deviations from the designed shape of the pole boundary.

Material Properties and Results of Machining

The material used for the pole plates is forged steel with the following chemical analysis: [5]

C(%)	Si(%)	Mn(%)	P(%)	S(%)	N(%)
0.02	0.22	0.40	0.02	0.013	0.009

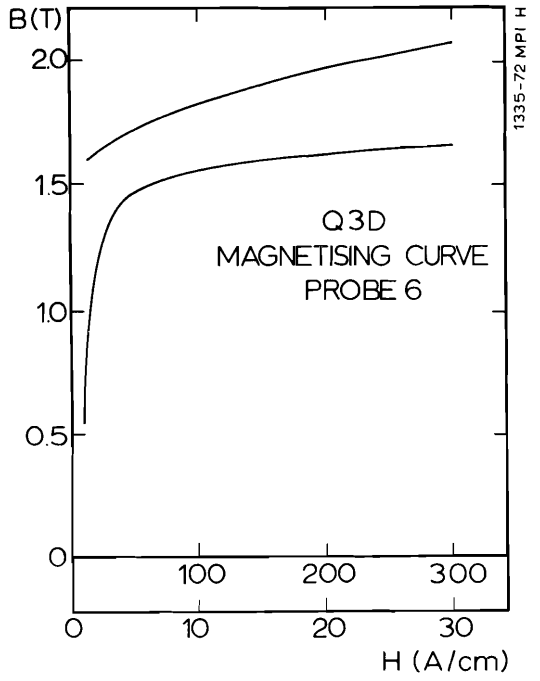

Fig.3. Magnetising curve of the pole piece material. Values for remanence and coercive force are B_r=11.9kG and F_c=0.85 A/cm.

Magnetising curves on this material have been made; a typical example is shown in Fig. 3 .

Detailed mappings of the mechanical tolerances revealed deviations from the designed pole shapes of less than 0.2 mm. The gap width of the magnets differed by not more than ± 0.005 mm from the expected 80 mm measured in a grid of 5 cm base length. To accomplish this, pole pieces have been partly handscraped after the final machining.

III. Field Mapping

Before assembly the components of the spectrograph have been mapped at various excitations. The excitation procedure was crucial for the uniformity and reproducibility of the field distribution, which is dealt with in another paper of this conference.[6] The homogeneous parts of the dipole magnets have been mapped with NMR probes, fringe fields and quadrupole by Hall probe measurements.

Homogeneous Parts of Dipoles

The excitation procedure yielding best uniformity was found to be the following. First the magnet is excited to 17 kG; with a speed of 80 G/sec the field is run down and the desired field "undershot" by 20% of the final setting, which is then approached at a rate of 40 G/sec. Figure 4 shows a typical field map of dipole 1. NMR - probe measurements were taken in a grid of app. 5 cm x 5 cm. The deviation from the average field level is shown cross-hatched for measurements across the magnet. Essentially the same results have been achieved for fields between 3 and 15 kG and also for dipole 2. The maximum deviation in a region 2.5 gap width away from the pole boundaries in no case exceeded $dB/B = \pm 1.5 \times 10^{-4}$

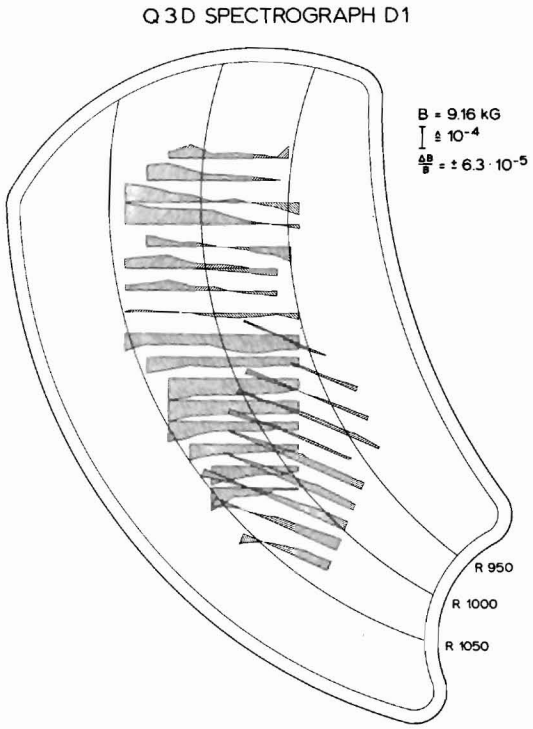

Fig. 4. Typical field map of dipole 1

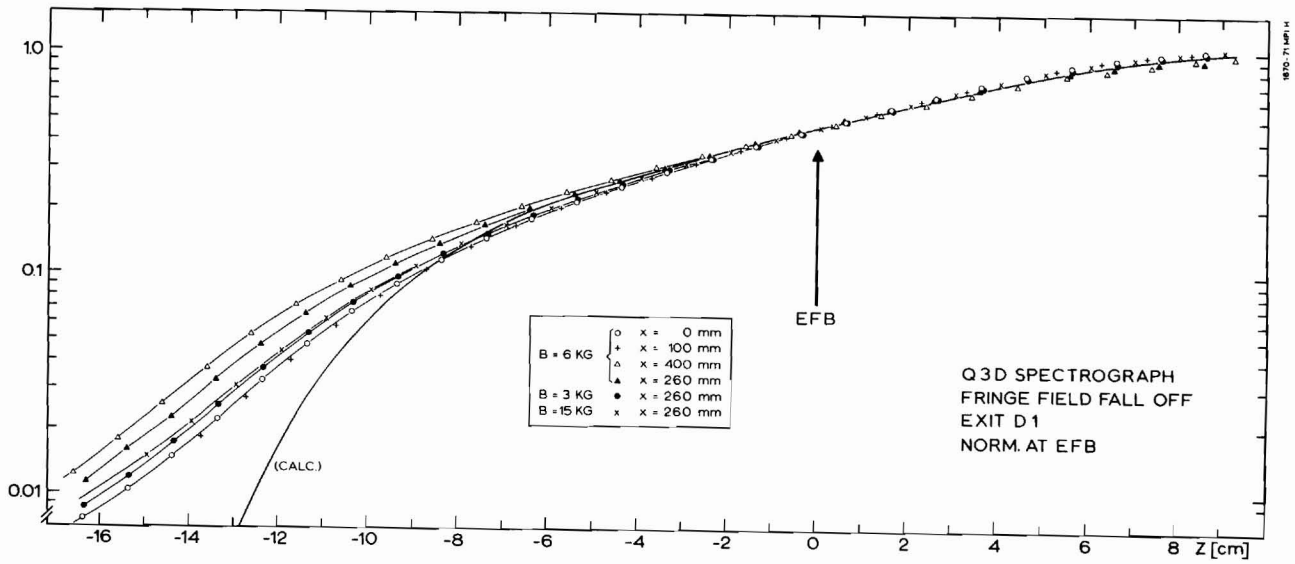

Fig. 5. Fringe field fall-off along different cuts at exit dipole 1

Fringe Fields

A field mapping machine with a positioning accuracy of about 0.2 mm and a Hall probe with a test accuracy of about 2 G has been used. The decay of the B_y - component in the median plane has been measured in a range of about ± 30 cm from the pole boundaries. The field clamps were mounted. Figure 5 shows the data from various cuts for the exit pole face of dipole 1. Also included is the fringe field decay as assumed in the design calculations. The curves are normalised to the position of the effective field boundary.

The fringing B_y field in the median plane is described by:[1]

$$B_y/B_o = (1 + e^S)^{-1},$$

where B_o denotes the uniform field deep inside the magnet and s measured along the normal to the pole boundary. Here S is a polynomial:

$$S = c_o + c_1 s + c_2 s^2 + c_3 s^3 + c_4 s^4 + c_5 s^5 .$$

TABLE III. Comparison of Measured Fringe Field Decay Coefficients C_o-C_5 to Design Coefficients for Exit D2.

Position	B_o(kG)	c_o	c_1	c_2	c_3	c_4	c_5
Exit D2	3	0.2612±0.003	1.7080±0.008	-0.4132±0.0165	0.6295±0.01	-0.2009±0.01	0.0172±0.003
	6	0.2639	1.7150	-0.4170	0.6300	-0.2043	0.0179
	12	0.2622	1.7176	-0.4098	0.6312	-0.2038	0.0118
Design		0.2049	1.6821	-0.5654	0.4004	0.0011	0.1663

TABLE IV. Comparison of Measured EFB Curvature Parameters to Design Parameter for Exit D2.

Position	B_o(kG)	RAP (cm^{-1})	CAT (cm^{-3})	CFV (cm^{-4})	CNN (cm^{-5})
Exit D2	3	$(-3.504\pm0.074)10^{-3}$	$(1.228\pm0.108)10^{-6}$	$(2.552\pm7.195)10^{-9}$	$(6.447\pm1.884)10^{-10}$
	6	$(-3.400\pm0.074)10^{-3}$	$(1.688\pm0.108)10^{-6}$	$(-6.720\pm7.189)10^{-9}$	$(2.026\pm1.883)10^{-10}$
	12	$(-3.397\pm0.074)10^{-3}$	$(1.836\pm0.108)10^{-6}$	$(-5.972\pm7.187)10^{-9}$	$(1.229\pm1.883)10^{-10}$
Design		$-3.37 \cdot 10^{-3}$	$2.1 \cdot 10^{-6}$	$-9.7 \cdot 10^{-9}$	$-2.5 \cdot 10^{-11}$

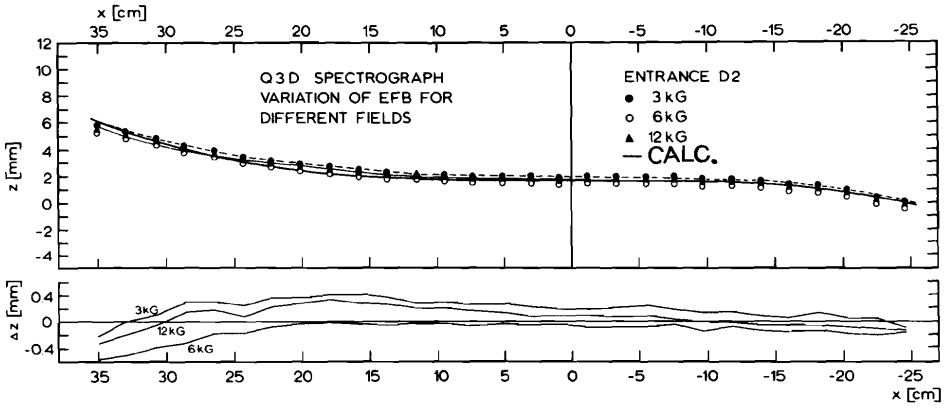

Fig. 6. Variation of EFB for different excitations for the pole face of dipole 2. The design EFB is normalized to the experimental data by a shift in z.

All measured fringe field curves for one pole face have been simultaneously fitted with this ansatz; coefficients $c1 \ldots c_5$ have been determined by a least squares fitting procedure. It turned out that coefficients higher than c_3 are very insensitive, the off-median plane should have been measured for a more accurate determination. Table III contains a comparison of experimental and design coefficients.

The coordinate a of the EFB is defined by

$$a = \int_0^{s1} B_y ds \; / \; B_o \; ,$$

if the point o is in the uniform region and s1 in the field free region. The shape of the EFB's have been determined for all pole faces at different excitations. Figure 6 shows an example, the z-axis is along the trajectories. Generally all magnets turned out to be wider than anticipated in the design for the normal field clamp positioning. The relative agreement, however, is such that experimental and design shape do not deviate by more than 0.2 mm, at most. The formula assumed in the ray tracing program for the shape of the pole boundary is in units of the gap width D [1].

$$s = \frac{1}{D}\left\{ \pm \left[(z+A)^2 + x^2 \right]^{\frac{1}{2}} - A \right\} + CAT\, x^3 + CFV x^4 + CNN x^5$$

where A = 1/RAP denotes the second order curvature of the pole boundary. Similarly the parameters CAT, CTV and CNN denote third- fourth- and fifth order corrections to it. The measured EFB positions have been fitted with this formula. Table IV contains the results and a comparison to the design parameters for the exit face of dipole 2, as an example. Again it turned out that CV and CNN are not very sensitively determined since only a part of the pole boundaries could be scanned due to limited access of the field mapping machine through the field clamps.

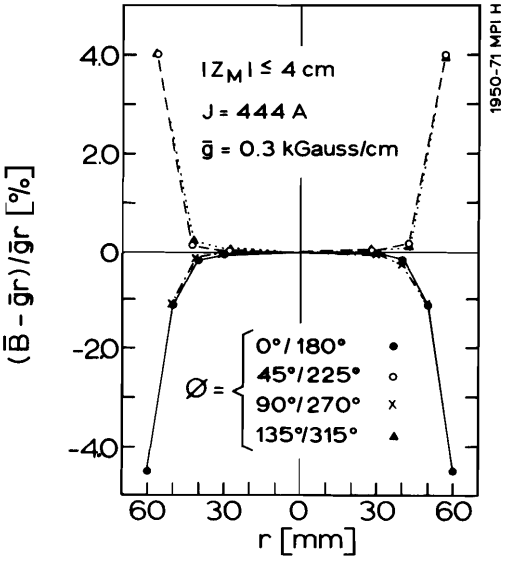

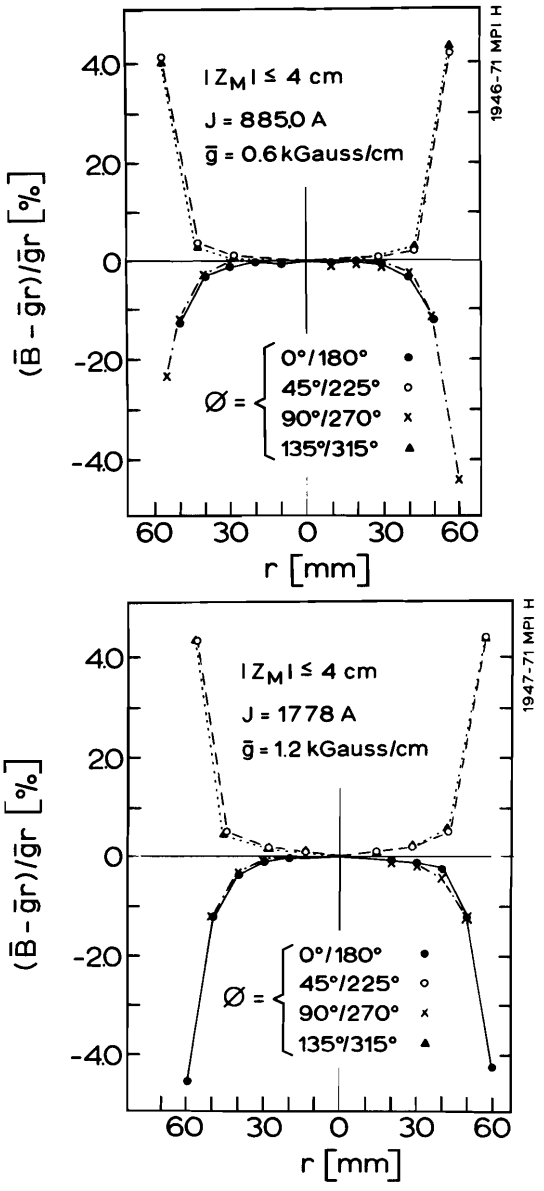

Fig. 7. Relative deviations from the pure quadrupole fields at different excitations.

Results of Quadrupole Mappings

The quadrupole singlet of the QDDD spectrograph has been scanned with the field mapping machine at DESY, Hamburg. Symmetries of the field and the possible admixtures of higher harmonic multipoles were investigated. The field cross section in the homogeneous region - at the center of the magnet and normal to the beam axis - is shown in Fig. 7 for different excitations.

The relative deviation $(\bar{B} - \bar{g}r)/\bar{g}r$ of the real quadrupole field from the ideal field $B_{id} = \bar{g}r$ is presented as a function of the

distance from the axis r, where $\bar{g}$ is the averaged gradient within $r \leq 3$ cm. The angle between the midplane of the spectrograph and the normal on the Hall probe is denoted by ϕ.

The deviations from the pure quadrupole field can be explained by relative admixtures of a dodecapole field of $P_{12} = -1.26 \cdot 10^{-9}$ and icosapole field of $P_{20} = 7.7 \cdot 10^{-17}$ (see Ref. 7). The sextupole and octupole strengths have been estimated to be lower than 10^{-4} and 10^{-5}.

The effective length has been determined, too, and was found to be only 28.9 cm instead of 30 cm in the design. The focussing power goes quadratically with the effective length and only linearly with the gradient. The quadrupole - which is connected in series with the dipoles to the power supply - has thus been provided with additional trim coils and an extra power supply. Due to limited space for the trim coils these at the moment limit the current, hence the maximum attainable pole tip field. New coils should replace the old ones in the near future.

Conclusions

The nonuniformities of the homogeneous are estimated to contribute less than $dp/p = 3.10^{-5}$ to the resolution. However, the different fringe field decay and the measured curvatures have remarkable effects. These parameters have thus been in turn inserted into a ray tracing program and line shapes have been calculated. Since only parts of the pole boundaries have been scanned these calculations reflect the expected line shapes for one half of the designed opening angle of the spectrograph. Figure 8 shows the line shapes, when successively the quadrupole asymmetries and the different curvatures of dipole 1 to 3 are taken into account.

The EFB can be shifted, when the field clamps are moved. The effect has been measured for different excitations and is shown in Fig. 9 for the exit pole face of dipole 1. According to these results the position of the field clamps have been altered substantially from the design.

IV. Experimental Ray-tracing

The design calculations have been done with 14 rays subtending filling the acceptance angle of the QDDD spectrograph[1]. The intersection of the axial ray with $\Theta=\emptyset=0$ mrad and the paraxial ray with $\Theta=\emptyset=1$mrad determine the first order focus. The remaining 12 ray are denoted in ref.1. The extreme rays used had a maximum angle in the dispersive plane of $\Theta = \pm 55$ mrad and in the axial plane of $\emptyset = \pm 63$ mrad. The spot size of the beam on target was 1mm wide and 1.5 mm high. A special collimator which opens one hole at a time has been built and mounted. Elastically scattered ^{3}He particles of E = 24 MeV and an estimated energy homogeneity of $dE/E = 10^{-4}$ have been used. Inside the detector chamber two solid state counters with dimensions 50 mm long and 5 mm high and a position resolution of dx = 0.3 mm (FWHM) have been mounted before and behind the expected focal plane. On five positions along the focal surface "stars" of the intersecting 14 rays have been measured and evaluated.

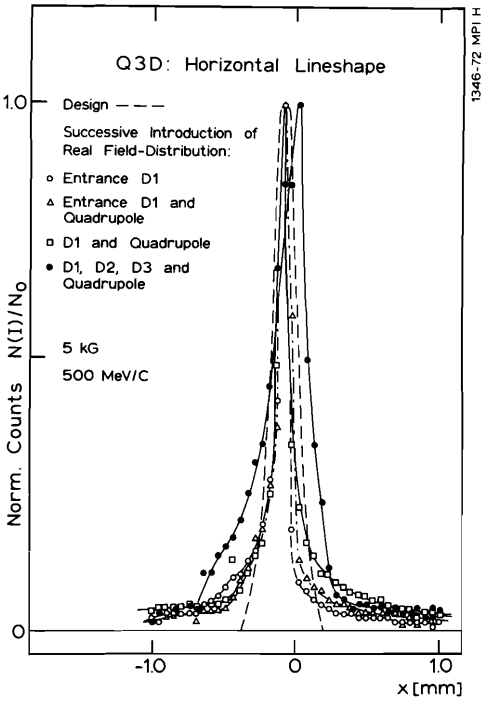

Fig. 8. Horizontal line shapes after introduction of real field - distribution.

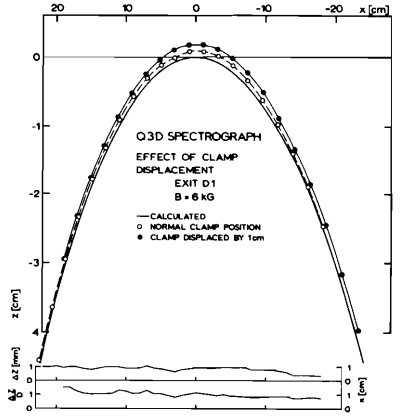

Fig. 9. Effect of clamp displacement on EFB at exit D1.

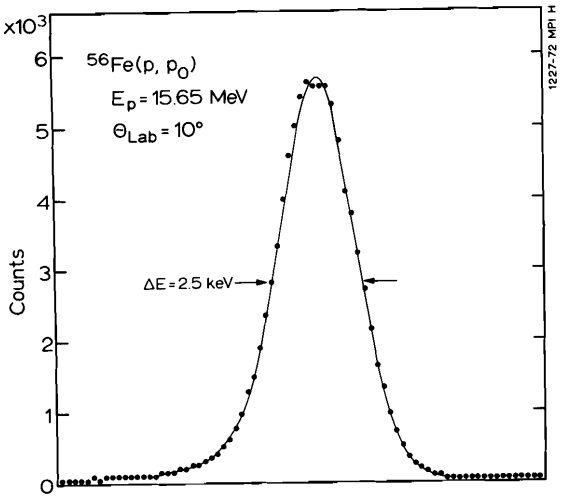

Fig. 10. Typical line shape for elastically scattered particles.

Results

The focal surface lies approximately 5 cm further towards the magnets for the range of bending radii investigated so far.

Aberration coefficients have been extracted from the stars at the first order focus. Table V shows a comparison between the main design aberrations and the experimental ones for the nominal radius ρ = 1 m.

TABLE V. Design And Experimental Aberration Coefficients

Aberrat. Coeff.	x/θ	x/θ^2	x/θ^3	x/θ^4
Design	-0.0023	-0.005	0.237	15.35
Exp.	0.0003	-0.281	1.6	153.8
Aberrat. Coeff.	x/ϕ^2	$x/\theta\phi^2$	$x/\theta^2\phi^2$	x/ϕ^4
Design	-0.02	-0.31	-11.17	-9.18
Exp.	0.02	-14.6	333.0	-16.9

The aberrations increase towards the ends of the focal plane; data are presently rechecked. The trend, however, can be seen from a comparison of the base widths of the stars at the focus (Table VI).

TABLE VI. Base Widths of the 14 Ray Stars

Bending Radius (cm)	104	102	100	98	96
Base width(cm)					
Design	0.17	0.19	0.08	0.09	0.16
Experiment	0.225	0.25	0.18	0.13	0.23

So far the field clamps have not been reshaped, which will be done to correct at least partly for the remaining aberrations. The QDDD spectrograph has been used for nuclear experiments already.[8] A typical line shape for elastically scattered particles is shown in Fig. 10.

Acknowledgements

The manufacturer of the QDDD spectrograph, Scanditronix (Stockholm) provided the data about the pole piece material. H.J. Scheerer participated in the field mappings of the dipole magnets. A.v.d. Decken, W. Saathoff, W. Reiter and W. Wannebohm analysed the data of the experimental ray tracing.

References

1. H.A. Enge and S.B. Kowalski, Proc. 3rd Int. Conf. on Magnet Technology, Hamburg, 1970, Edit. Commit. MT3 Desy (A. Curtze KG, Hamburg, 1970) p. 366.
2. H.A. Enge, Proc. of 1st Int. Conf. on Magnet Technology, Stanford, 1965, H. Brechna and H.S. Gordon, Editors (Stanford University, Stanford, 1965), p. 84.
3. K.L. Brown and S.K. Howry, Transport/360: A Computer Program for Designing Charged Particle Beam Transport Systems, SLAC Rep. No. 91, Stanford (1970).
4. V.D.I. Nachrichten, Jahrgang 26, Vol. 27 (1972), p. 9.
5. Scanditronix, Private Communication.
6. H.A. Enge, S.B. Kowalski, C.A. Wiedner M. Goldschmidt, and H. J. Scheerer; contribution to this conference.
7. K. Steffen, High Energy Beam Optics (J. Wiley Sons, N.Y., 1965), 1st ed., Vol. 17, p. 48.
8. A.v.d. Decken et al., submitted to Phys. Lett.